ISSN 0036-0236, Russian Journal of Inorganic Chemistry, 2023, Vol. 68, No. 3, pp. 334–341. © Pleiades Publishing, Ltd., 2023.
ISSN 0036-0236, Russian Journal of Inorganic Chemistry, 2023. © Pleiades Publishing, Ltd., 2023.
Russian Text © The Author(s), 2023, published in Zhurnal Neorganicheskoi Khimii, 2023, Vol. 68, No. 3, pp. 393–400.

SYNTHESIS AND PROPERTIES OF INORGANIC COMPOUNDS

Synthesis of Hydroxylapatite Substituted with REE Ions (La^{3+} and Y^{3+}): Composition, Structure, and Properties

O. A. Golovanova*

Omsk State University, Omsk, 644077 Russia

**e-mail: golovanoa2000@mail.ru*

Received August 2, 2022; revised October 3, 2022; accepted October 7, 2022

Abstract—Substituted hydroxylapatites (HAs) containing various La^{3+} or Y^{3+} percentages were prepared. X-ray powder diffraction, Four-transform IR spectroscopy, and optical spectroscopy verified the formation of substituted hydroxylapatites (La–HA and Y–HA). Inductively coupled plasma atomic emission spectrometry (ICP–AES) verified the presence of REE ions in the solids. Changes in the unit cell parameters of the prepared phases indicated that the REE ions substituted for Ca^{2+} ions in the hydroxylapatite structure. The lanthanum or yttrium percentage in precipitates increased in response to increasing REE salt concentration (within 1–5 wt %) in the initial solution as shown by chemical analysis; this brought about a decrease in the ratio Ca/P compared to the stoichiometric ratio (1.67). The solubility of the synthesized samples was studied, and it appeared that the cation-substituted hydroxylapatites were less soluble than undoped HA was.

Keywords: lanthanum and yttrium, ratio Ca/P, solubility

DOI: 10.1134/S0036023622700139

INTRODUCTION

Rare-earth elements (REEs) are not known as biometals, but their ions can exhibit biological activity. Some REE salts are used in the treatment of some diseases; their radioactive isotopes are capable of exerting an anti-cancer effect by acting on malignant tumors [1–3]. Rare-earth compounds may interfere with blood clotting to prevent blood clots and have anti-inflammatory properties. Rare-earth ions are not aggressive when exposed to the human body, for they do not have oxidizing properties; moreover, they have hydrated shells, which reduce their activity [5–8].

Lanthanide salts, their complexes and nanoparticles succeed in the treatment of bone diseases. The incorporation of lanthanide ions into the structure makes hydroxylapatite (HA) promising for use in bone materials engineering, specifically, changing its antimicrobial activity. Substitutions appreciably affect the structure, solubility, and thermal stability [9–11].

With the increasing number of bone diseases, tens of thousands of implants and endoprostheses are used annually in medicine; they are categorized into bioinert and bioactive ones. The latter comprise two types of calcium phosphate-based materials: hydroxylapatite and β-tricalcium phosphate, both having good biocompatibility, bioresorbability, and osteoinductivity with the human skeleton. Undoped HA, as a rule, is not used in implants, since it is a brittle material and has a low degree of osteoinduction; i.e., it poorly activates the formation of new bone tissue. Therefore, the material used in practice is HA doped with metal ions, which enter the HA structure to change its properties, specifically its bioactivity and bioresorbability [12–16].

Lanthanide-doped HA nanoparticles can be used as fluorescent labels, and they can become an alternative to organic fluorophores as they are more stable and have longer lifetimes. Such materials make it possible to study tissues in surgery, bone engineering, and for tissue repair [17, 18].

Lanthanides are known for their high affinity to HA. This is due to the lanthanide ions (Ln^{3+}) having ionic radii close to the Ca^{2+} radius; their biological activity is related to this fact. Rare-earth elements inhibit the formation of osteoclast-like cells and bone resorption. In addition, lanthanides have biological effect on the body to inhibit the growth of bacteria and change the structure of the outer cell membranes, which are responsible for cell permeability [2, 19].

The La^{3+}-doped HAs, for example, has a high strength and supports osteoblast adhesion; Y^{3+}-doped HAs are biocompatible, support cell proliferation, promote accelerated fibroblast growth and better osteoblast adhesion compared to the respective properties of unsubstituted hydroxylapatite [19, 20].

The goal of this work was to prepare and study hydroxylapatites doped with REE ions (La^{3+} and Y^{3+}).

EXPERIMENTAL

Synthesis

Hydroxylapatite samples were prepared by wet-chemistry methods [21]. The chemicals used to prepare initial solutions were pure for analysis grade calcium nitrate $Ca(NO_3)_2$ and ammonium hydrogenphosphate $(NH_4)_2HPO_4$ and aqueous NH_4OH solution. The synthesis was carried out at 23–25°C in accordance with the equation below:

$$10Ca(NO_3)_2 + 6(NH_4)_2HPO_4 + 8NH_4OH \rightarrow Ca_{10}(PO_4)_6(OH)_2 + 20NH_4NO_3 + 6H_2O.$$

To a 250-mL portion of 0.136 mol/L $Ca(NO_3)_2$ solution, dropped was (at a rate of 4.5–5.0 mL/min) a 250-mL portion of 0.080 mol/L $(NH_4)_2HPO_4$ solution, to which concentrated aqueous ammonia (5 mL) had been added beforehand, under vigorous stirring. Afterwards, pH in the thus-prepared solution was adjusted to 9.00 ± 0.05, and the solution was allowed to crystallize for 7 days. The precipitate was filtered off with a water jet pump, and the filtrate was stored for chemical analysis. The precipitate was washed with distilled water (V = 50 mL) and ethanol to improve the dispersion, dried in an oven at ~110°C for 24 h, crushed with a mortar and a pestle, and then placed in a desiccator to remove the remaining unbound water. Next, the resulting powder was transferred into a labeled bottle and weighed. Rare-earth-doped hydroxylapatites were prepared as described above using inorganic calcium and phosphorus salts. The La^{3+} and Y^{3+} ions were entered into the solution as well-soluble compounds: $La(NO_3)_3{\cdot}6H_2O$ and $Y(NO_3)_3{\cdot}6H_2O$.

Two experiments were carried out. In one experiment, $La(NO_3)_3{\cdot}6H_2O$ was used; in the other, $Y(NO_3)_3{\cdot}6H_2O$ was. In order to prepare REE-doped hydroxylapatites (REE/(REE + Ca^{2+}) of 1 to 5 wt % with 1% steps), a solution containing $Ca(NO_3)_2$ was added with a 0.1 M REE solution in the amount that would provide the set percentage.

Next, to the $Ca(NO_3)_2$ solution then containing REE ions (La^{3+} or Y^{3+}), an $(NH_4)_2HPO_4$ solution was dropped (at a rate of 4.5–5.0 mL/min) under vigorous stirring; the thus-prepared solution was brought to the set value of pH (9.00 ± 0.05) and then allowed to crystallize for 7 days.

The precipitate was crushed with a mortar and a pestle, and placed in a desiccator to remove the remaining unbound water. Afterwards, the resulting powder was transferred to a labeled bottle and then weighed.

X-ray powder diffraction analysis was performed by the Debye–Scherrer method on a DROM-3 diffractometer (CuK_α radiation, λ = 0.154 nm, 2θ angle range: 5°–60°).

The spectra were first processed with the DIFWIN 1 (https://www.updatestar.com/ru/topic/difwin) software suite. The recorded X-ray diffraction patterns were used to determine Bragg reflection angles and their relative intensities. The phase composition of the prepared samples was determined by qualitative and quantitative analyses with the MATCH! 3 software, in which the interplanar distances and relative intensities of diffraction peaks for each phase were compared to the respective values from the file [22].

The X-ray diffraction patterns of phases were used to calculate crystallite sizes by the Debye–Scherrer relationship:

$$d = \frac{k\lambda}{\beta\cos\theta},$$

where d is the crystallite size; k is the Scherrer constant, which is the particle form factor; λ is the wavelength; β is the peak width at half-height; and θ is the diffraction angle.

The X-ray diffraction patterns were used to calculate the unit cell parameters of samples in the software "Spreadsheet Processor for X-ray Structure Analysis" (RTP), in the natural minerals network database (Mineralogy Database, http://webmineral.com).

Fourier-transform IR spectra were recorded on an FSM-2202 spectrophotometer. Test samples to record a spectrum were prepared as follows: a powder sample was blended with a KBr powder in the ratio 1 : 100, then the mixture was compacted on a tablet press, and the tablet was placed to the spectrophotometer cell. The software used was FSPEC, the recording range was from 400 to 4000 cm^{-1}, and the total number of scans was 32. The software used to process the spectra was ORIGIN 2021.

The morphology of solids was studied using an XSZ-107 microscope and a TOUPCAM video eyepiece at 160× magnification. Micrographs were obtained using the TOUPVIEW program.

The cations in the solid phases of the prepared samples were determined by inductively coupled plasma atomic emission spectrometry (ICP-AES) [23]. Calibration solutions were prepared via successive dilution of the standard solution. Solutions were injected into the plasma in the following order: the zero solution, then calibration solutions in the ascending order of concentrations, blank solution, and test solution. After all solutions were analyzed, the background correction was applied using software.

The stability to electrolytes was studied on samples dissolved in 0.01 M HCl (pH 2) and in acetate buffer (pH 5.5). The process was carried out under vigorous stirring at T = 298 K; the change in Ca^{2+} concentration (pCa) and pH were recorded on an I-160MI ion meter in certain time intervals (τ = 0–40 min in 1-min intervals). The thus-gained data were used to plot pCa = $f(\tau)$ and pH = $f(\tau)$ kinetic curves and to calculate the dissolution rates of the samples [24].

In supernatant liquids after the solid was completely separated, pH and Ca^{2+} concentration were measured potentiometrically. Residual phosphate ions in the solution were determined photometrically as molybdenum blue (RD 52.24.382-2006, regulatory documents on the determination of "weight concentrations of phosphates and polyphosphates") on a KFK-2 device.

La^{3+} and Y^{3+} Determination in Acid Solution with Arsenazo(III)

The La^{3+} and Y^{3+} were determined on a YuNIKO-1201 spectrophotometer at the wavelength $\lambda = 650$ nm, the cell thickness $l = 3$ cm, and pH 1.8–2.0. Three replicate measurements were done, and the average optical densities were used to plot the $d = f(c(REE))$ calibration plot.

RESULTS AND DISCUSSION

Figure 1a shows the X-ray diffraction patterns of undoped HA samples and La^{3+}-doped HAs. One can see that the prepared phase is hydroxylapatite. The X-ray diffraction pattern features reflections at 25.8° (002), 28.9° (210), 31.8° (211), 32.9° (300), and 34.0° (202), which verifies the presence of a hydroxylapatite phase in the REE-free sample. The La^{3+}-doped samples have X-ray diffraction patterns similar to the X-ray diffraction pattern of the REE-free hydroxylapatite, but with the characteristic angles shifting toward the higher values. This observation can signify the isomorphic substitution of La^{3+} (1.17 Å) for Ca^{2+} (1.14 Å) in the HA structure and an attendant distortion of the crystal lattice and its parameters [11].

Figure 1b shows the X-ray diffraction patterns of undoped HA and the HA samples synthesized in the presence of Y^{3+}. The X-ray diffraction patterns are similar to one another; that is, they refer to a hydroxylapatite phase. The X-ray diffraction patterns of the Y^{3+}-doped samples feature shifts of characteristic angles, which can serve as a signature of the substitution of Y^{3+} (1.12 Å) for Ca^{2+} (1.14 Å) in the hydroxylapatite structure.

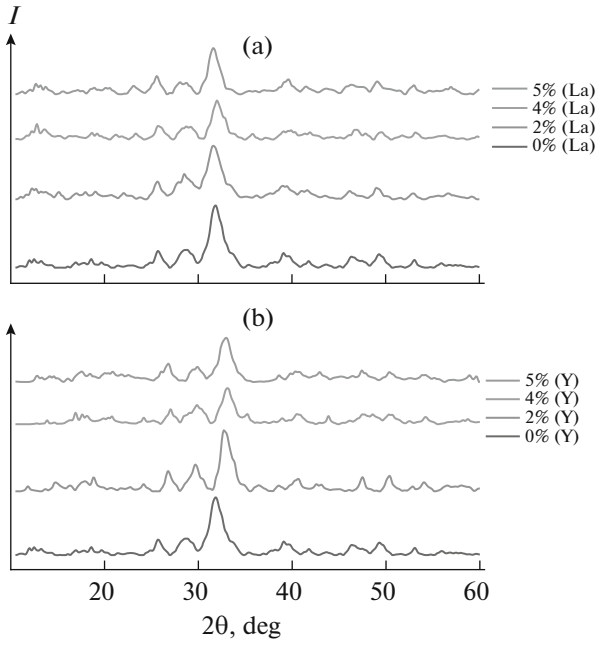

Fig. 1. X-ray diffraction patterns of (a) La^{3+}-doped and (b) Y^{3+}-doped hydroxylapatite samples.

The measured X-ray diffraction patterns were used to calculate the unit cell parameters for the synthesized samples (Table 1).

The contents of Table 1 imply that La–HA and Y–HA have greater unit cell parameters than those of unsubstituted HA. A greater increase in the parameter *a* compared to the parameter *c* is because lanthanum ions prefer to occupy the Ca(2) position in the hydroxylapatite structure [1, 3]. The Y–HA unit cell parameters change to a lesser extent than the La–HA parameter because of the smaller difference between the yttrium and calcium ionic radii than between the lanthanum and calcium ionic radii. One-way ANOVA analysis using the STATIC 2 program showed that, for

Table 1. Unit cell parameters

Sample	$\frac{C_{REE}}{C_{REE} + C_{Ca}}$, %	Unit cell parameters, nm	
		$a \pm 0.001$	$c \pm 0.001$
HA	–	0.944	0.689
La–HA	2%	0.948	0.694
	4%	0.951	0.695
	5%	0.960	0.699
Y–HA	2%	0.945	0.690
	4%	0.947	0.692
	5%	0.948	0.693

C_{REE} is the REE ion concentration; C_{Ca} is calcium ion concentration, wt %.

Table 2. Mean crystallite sizes

$D_{mean} \pm 0.03$ nm		
$\frac{C_{REE}}{C_{REE} + C_{Ca}}$, %	La^{3+}	Y^{3+}
0	0.31	0.31
2	0.31	0.30
4	0.31	0.30
5	0.32	0.30

all doped samples, the factor was statistically significant compared to undoped HA.

The X-ray diffraction patterns were used to calculate mean crystallite sizes by the Debye–Scherrer relationship (Table 2). Clearly, the compounds were nanocrystalline, which rises their potential for use in medicine, e.g., for targeted delivery of drugs, and REE ion additives, as a rule, did not affect the crystallite size of the synthesized samples. One-factor analysis of variance was carried out using the STATIC 2 program, and showed that the factor was not statistically significant. The discrepancy between the samples in terms of the mean value was statistically insignificant.

Fourier-transform IR spectroscopy was used to determine the group composition of samples. Figure 2a shows the spectra of REE-free hydroxylapatite and of samples containing various amounts of La^{3+} or Y^{3+}. The broad band at 3340–3600 cm^{-1} relates to the bending vibrations in OH^- groups; the band in region of 1590–1690 cm^{-1} is due to the H–O–H bending vibrations in the H_2O structure. Low-intensity stretching vibrations appear in the region of 1360–1410 cm^{-1} corresponding to the P=O bond, and a broad strong band appears in the range 900–1100 cm^{-1} relating to the P–O stretching vibrations; and the P–O–P bending vibrations appear at 550–620 cm^{-1}. The spectrum also features bands at 880, 960 (ν_2), 1080 (ν_3), and 565 (ν_4) cm^{-1} relating to the vibrations in PO_4^{3-}. Noteworthy, the spectra have similar patterns.

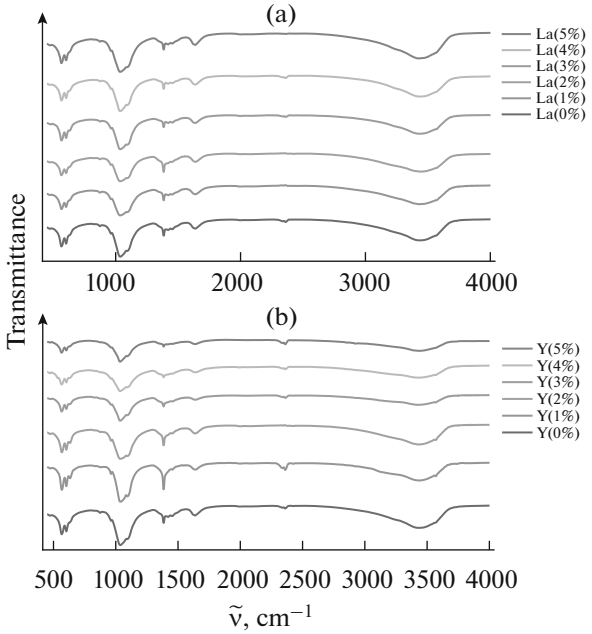

Fig. 2. IR spectra of (a) La^{3+}-doped and (b) Y^{3+}-doped hydroxylapatite samples.

In some IR spectra, a band is observed in the region of 2300–2400 cm^{-1} due to the vibrations in CO_3^{2-}. The carbonate ions appear in the HA structure due to the carbon dioxide absorbed by hydroxylapatite from the air during the synthesis, as a result of which CO_3^{2-} ions can occupy the phosphate ion (B-type) positions in the structure. The IR spectra of all prepared samples are alike; this signifies that substitutions occur in the cationic, and not anionic, position in the HA structure.

The as-synthesized solid phases were studied by optical microscopy in order to elucidate their morphology. Micrographs (Fig. 3a) show that REE-free HA crystals have irregular-shaped faces; sharp cleaves are observed, but the particles yet have clear-cut edges and a small spread in size. The REE-doped samples, as a rule, have crystals with less clear edging. Clear-cut edging appears in samples with 5% additives (Figs. 3c and 3e); such changes in particles characterize the isomorphic incorporation of the REE into the hydroxylapatite structure.

Particle aggregation is typical of the REE-doped samples; that is, REE additives in the form of ions help aggregation, and this effect is more pronounced in the 5% REE samples. This behavior is explained by the agglomeration of particles with uncompensated charges upon the isomorphic substitution of calcium ions in the HA structure by REE(+3) ions.

The amounts of REE ions in solid samples were determined and calculated by ICP-AES. The results of chemical analyses and ICP-AES served us to suggest structural formulas of the prepared doped hydroxylapatite samples (Table 3).

It can be seen that REE ions, introduced as a percentage of calcium, almost completely enter the solid phase and substitute for calcium ions in the hydroxylapatite structure to form La–HA and Y–HA doped solid phases.

The calcium ion, phosphate ion, and REE concentrations were determined by chemical analyses (Table 4). These concentrations showed that the ratio Ca/P, which is an important characteristic of synthesized samples, is smaller for the REE-substituted HAs. The REE concentrations determined by chemical analyses in the solution after the precipitate was separated ver-

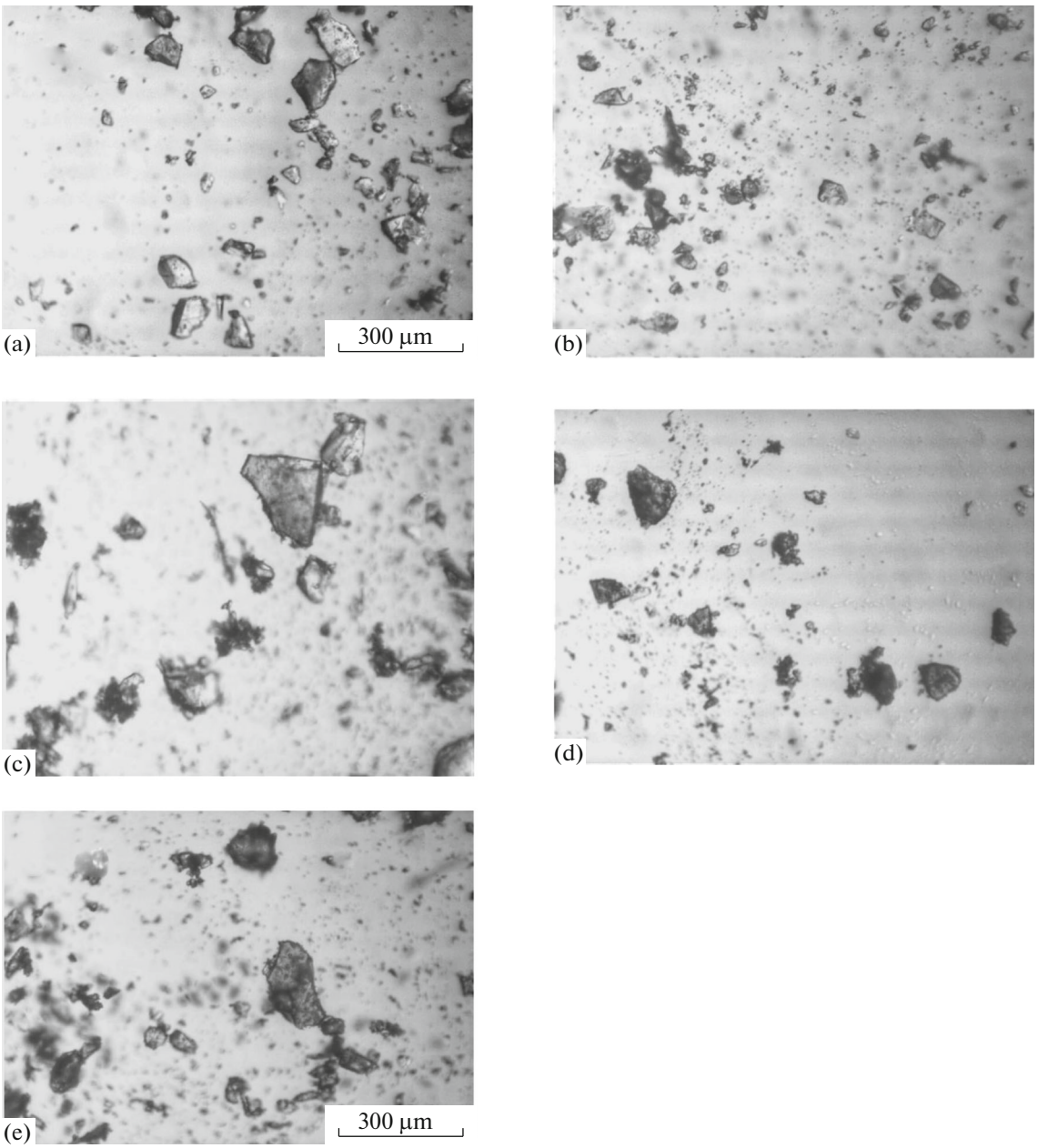

Fig. 3. Micrographs of HA samples: (a) REE-free and (b–e) doped with (b) 2% La^{3+}, (c) 5% La^{3+}, (d) 2% Y^{3+}, and (e) 5% Y^{3+}.

ify that the REE ions are incorporated into the solid phase. The amount of REE ions in the precipitate increases as the REE concentration in the initial solution rises.

Thus, the ratio Ca/P in the prepared compounds is lower than the stoichiometric value typical of hydroxylapatite, equal to 1.67. This observation confirms the occurrence of isomorphic substitution of REE ions for

Table 3. ICP-AES results

$\frac{C_{REE}}{C_{REE}+C_{Ca}}$ (calcd.), %	REE ion concentration in solution, μmol/L	$\frac{C_{REE}}{C_{REE}+C_{Ca}}$ (exp.), %	Formula
La^{3+}, 5	3.4 ± 0.1	4.7	$La_{0.47}Ca_{9.53}(PO_4)_6(OH)_{2.47}$
Y^{3+}, 5	3.6 ± 0.1	4.9	$Y_{0.49}Ca_{9.51}(PO_4)_6(OH)_{2.49}$

Table 4. Percentages of ions in the solid phases of synthesized HA samples

$\frac{C_{REE}}{C_{REE}+C_{Ca}}$ (calcd.), %	$\frac{C_{REE}}{C_{REE}+C_{Ca}}$ (exp.), %		Ca/P ± 0.01	
	La^{3+}	Y^{3+}	La^{3+}	Y^{3+}
1.0	0.9	1.0	1.62	1.61
2.0	1.8	1.9	1.59	1.59
3.0	2.8	3.0	1.57	1.57
4.0	3.6	3.8	1.56	1.56
5.0	4.7	4.9	1.55	1.54

Ca^{2+} ions in the HA structure. Goldschmidt's rule states that isomorphism is possible only when the difference between the radii of the interchanging ions does not exceed 15%. Comparing the Ca^{2+} radius (1.14 Å) and the Goldschmidt radii of La^{3+} (1.17 Å) and Y^{3+} (1.12 Å) substituents, we can see that they have close values and their difference does not exceed 15%. Thus, we can conclude that these ions satisfy Goldschmidt's rule and their isomorphism is possible [25, 26].

Bioactivity is an important characteristic of hydroxylapatite-based materials. While the material dissolves, inorganic ions leave its structure and contribute to the formation of the inorganic component of the bone matrix, which favors the formation of bone tissue.

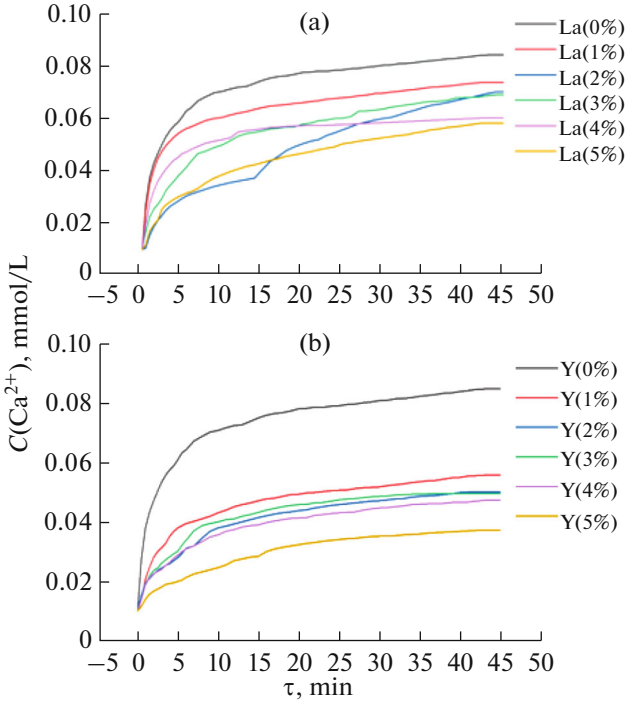

Fig. 4. Dissolution rate curves in acetate buffer for (a) La^{3+}-doped and (b) Y^{3+}-doped hydroxylapatite samples.

The prepared samples were dissolved in acetate buffer (pH 4.5) and in 0.01 M hydrochloric acid (pH 2.0).

The plotted $C(Ca^{2+}) = f(\tau)$ kinetic curves (Fig. 4) imply that saturation with calcium ions occurs approximately in the 15th minute post dissolution. The HA prepared without addition of REE ions has a higher solubility than that of samples with REE additives. The solubility of HA becomes lower when the REE enters the crystal lattice. This can arise from the mutual influence of Ca^{2+} and REE ions, which increases the unit cell parameters of HA and decreases its solvability and proneness to dissociation.

In addition, there is an energy gain for La–HA and Y–HA isomorphic compounds. According to Fersman's law of diagonal isomorphism, the energy gain takes place if an ion of the same (or close) size and of the same sign, but of a higher charge, enters the crystal lattice instead of a low-charge ion. The second reason lies in the surface adsorption of phosphate ions due to an incomplete compensation of positive charges upon isomorphic substitution.

Thus, the synthesized HAs that contain La^{3+} or Y^{3+} can inhibit or suppress the activity of osteoclasts and thereby prevent bone destruction. Accordingly, the material based on REE-doped HA may have beneficial effects when used in bone engineering.

Various trends were observed when the solubility of the prepared samples was studied in hydrochloric acid (pH 2.0), which models active resorption. The solution saturates with calcium ions at the 10th minute. The La^{3+}-doped HA samples, for example, are dissolved at a lower rate than REE-free HA is (Fig. 5a), while HA samples doped with 1% Y^{3+} have a higher dissolution rate compared to undoped hydroxylapatite. Therefore, HAs containing Y^{3+} ions (1 wt %) in their structures can favor the resorption of the material.

Kinetic data processing using the data sampling technique showed the zero order of dissolution reactions, which is typical of heterogeneous reactions. In view of this, the dissolution reaction rates were calculated using the appropriate equation [24, 27] (Table 5).

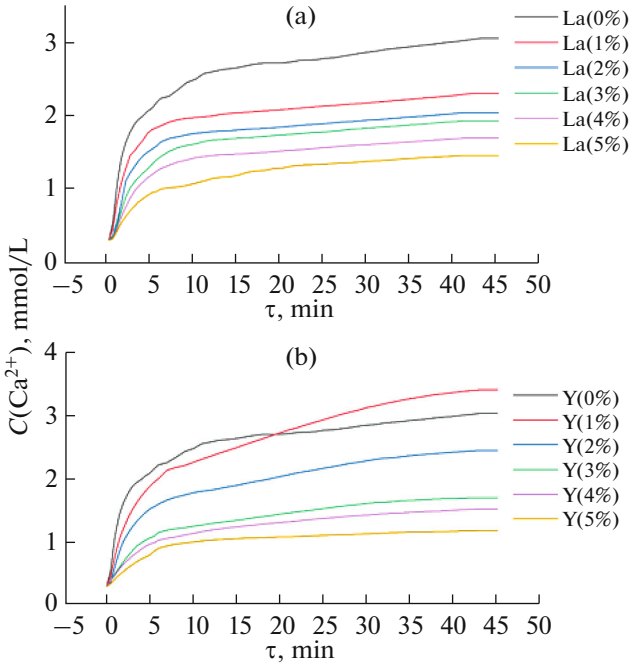

Fig. 5. Dissolution rate curves in HCl for (a) La^{3+}-doped and (b) Y^{3+}-doped hydroxylapatite samples.

Dissolution in acetate buffer exhibited a common trend: the dissolution rate of undoped HA is higher than that of REE-doped HAs; La–HA (1%) and Y–HA (1%) have the highest dissolution rates.

Dissolution in HCl showed that the degradation rate of the substituted samples was lower than that of the HA prepared without additive ions. Of the substituted samples, Y–HA had the highest dissolution rate (1%). The dissolution process also featured the following trend: the greater the amount of REE ions incorporated into the HA structure, the lower the HA dissolution rate.

Comparing dissolution rates in various solvents, one can see that the process rate is higher in HCl solutions because of their high acidity.

Table 5. Dissolution rates of synthesized samples

REE ion additive, %		$V \times 10^{-5}$, mol/(L min)	
		acetate buffer	HCl
0		2.78	9.90
La^{3+}	1	2.34	7.34
	2	2.05	6.38
	3	1.94	5.94
	4	1.74	5.05
	5	1.59	4.06
Y^{3+}	1	1.63	10.4
	2	1.46	7.39
	3	1.41	4.85
	4	1.31	4.26
	5	1.05	3.24

CONCLUSIONS

Substituted hydroxylapatites containing various amounts of La^{3+} or Y^{3+} (1–5% with 1% steps) have been prepared. The formation of La–HA and Y–HA substituted hydroxylapatites with various concentrations of dopant ions has been verified. The increasing batch concentrations of REE-containing reagents in the range 1–5% brought about an increase in their concentrations in the precipitates and, thereby, a decrease in the ratio Ca/P (1/67). The cation-substituted hydroxylapatites have been found to be less soluble than undoped hydroxylapatite. Such compounds can inhibit and suppress the action of osteoclasts, thereby preventing the destruction of bone tissue and maintaining its integrity. Accordingly, materials based on REE-doped hydroxylapatites can be used in bone engineering.

CONFLICT OF INTEREST

The authors declare that they have no conflicts of interest.

REFERENCES

1. K. Kulwinder, K. J. Singh, V. Anand, et al., Ceram. Int. **43**, 10097 (2017). https://doi.org/10.1016/j.ceramint.2017.05.029
2. K. Wieszczycka and K. Staszak, Wózniak-Budych, et al., Coord. Chem. Rev. **388**, 248 (2019). https://doi.org/10.1016/j.ccr.2019.06.017
3. A. Szcześ, L. Hołysz, and E. Chibowski, Adv. Colloid Interface Sci. **249**, 321 (2017). https://doi.org/10.1016/j.cis.2017.04.007
4. A. D. Furasova, A. F. Fakhardo, V. A. Milichkoet, et al., Colloids Surf., B: Biointerfaces **154**, 21 (2017). https://doi.org/10.1016/j.colsurfb.2017.02.029
5. A. A. Sherstiuk, S. A. Tsymbal, A. F. Fakhardo, et al., ACS Biomater. Sci. Eng. **7**, 5633 (2021). https://doi.org/10.1021/acsbimaterials.1c00973
6. V. O. Vasylechko, G. V. Gryshchouk, V. P. Zakordonskiy, et al., Talanta **162**, 1 (2017). https://doi.org/10.1016/j.talanta.2017.06.052
7. C. Shen, T. Yan, Y. Wang, et al., J. Lumin. **10**, 1 (2017). https://doi.org/10.1016/j.jlumin.2016.12.018
8. C. Boronat, T. Rivera, J. Garcia-Guinea, et al., Radiat. Phys. Chem. **130**, 236 (2017). https://doi.org/10.1016/j.radphyschem.2016.09.005
9. S. George, D. Mehta, and V. K. Saharan, Rev. Chem. Eng. **36**, 369 (2020). https://doi.org/10.1515/revce-2017-0101

10. T. R. Machadoa, J. C. Sczancoskia, H. Beltran-Mirb, et al., Ceram. Int. **44**, 236 (2018). https://doi.org/10.1016/j.ceramint.2017.09.164
11. P. E. Kazin, M. A. Pogosova, L. A. Trusov, et al., J. Solid State Chem. **237**, 349 (2016). https://doi.org/10.1016/j.jssc.2016.03.004
12. N. Nasiri and C. Clarke, Biosensors **9**, 43 (2019). https://doi.org/10.3390/bios9010043
13. G. A. Shashkina and V. F. Sorets, Med. Ekstremal. Sit. **1**, 101 (2017).
14. Ma Guoqing, Mater. Sci. Eng. **688**, 1 (2018). https://doi.org/10.1088/1757-899X/688/3/033057
15. X. Zheng, M. Liu, J. Hui, et al., Phys. Chem. Chem. Phys. **17**, P. 20301 (2015). https://doi.org/10.1039/c5cp01845e
16. L. I. Ardanova, E. I. Get'man, S. N. Loboda, et al., Inorg. Chem. **49**, 10687 (2010). https://doi.org/10.1021/ic1015127
17. I. A. Neacsu, A. E. Stoica, B. S. Vasile, et al., Nanomaterials **9**, 239 (2019). https://doi.org/10.3390/nano9020239
18. Yu. O. Nikitina, N. V. Petrakova, A. Yu. Demina, et al., Russ. J. Inorg. Chem. **66**, 1067 (2021). https://doi.org/10.31857/S0044457X21080171
19. J. F. Cawthray, A. L. Creagh, C. A. Haynes, et al., Inorg. Chem. **54**, 1440 (2015). https://doi.org/10.1021/ic502425e
20. G. D. Sathishkumar and A. S. Karthika, et al., Ind. Eng. Chem. Res. **53**, 20145 (2014). https://doi.org/10.1021/ie504387k
21. A. P. Solonenko and O. A. Golovanova, Russ. J. Inorg. Chem. **59**, 1228 (2014). https://doi.org/10.1134/S0036023614110230
22. Yu. K. Egorov-Tismenko, *Crystallography and Crystal Chemistry* (Moscow, 2014) [in Russian].
23. M. Thompson and J. N. Walsh, *A Handbook of Inductively Coupled Plasma Spectrometry* (Blackie, Glasgow and London, 1983).
24. A. A. Tsyganova and O. A. Golovanova, Inorg. Mater. **55**, 1156 (2019). https://doi.org/10.1134/S0020168519110141
25. V. S. Urusov and N. N. Eremin, *Crystal Chemistry* (Izd-vo Mosk. Univ., Moscow, 2005) [in Russian].
26. T. Tite, A. C. Popa, L. M. Balescu, et al., Materials **11**, 2081 (2018). https://doi.org/10.3390/ma11112081
27. O. A. Golovanova, Russ. J. Inorg. Chem. **65**, 305 (2020). https://doi.org/10.1134/S0036023620030043

Translated by O. Fedorova